Article

Immunity

Spatiotemporally Distinct Interactions with Dendritic Cell Subsets Facilitates CD4+ and CD8+ T Cell Activation to Localized Viral Infection

Graphical Abstract

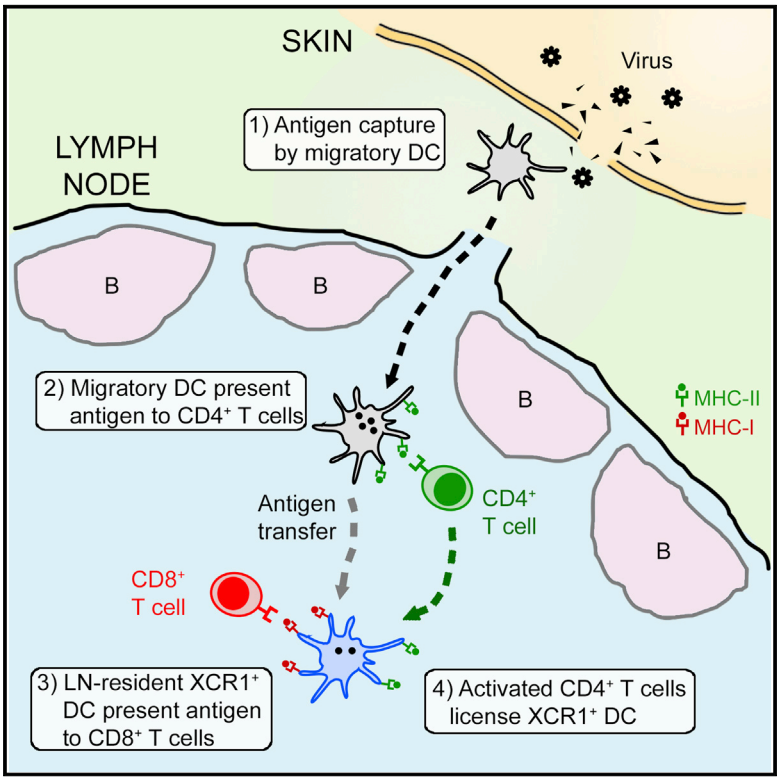

Highlights

- Activation of T cell subsets after peripheral virus infection is temporally regulated
- $CD4^+$ T cells, but not $CD8^+$ T cells, are activated early by migratory DCs
- $CD8^+$ T cell activation is delayed until LN-resident $XCR1^+$ DCs can prime
- $XCR1^+$ DCs are critical for the delivery of T cell help

Authors

Jyh Liang Hor, Paul G. Whitney, Ali Zaid, Andrew G. Brooks, William R. Heath, Scott N. Mueller

Correspondence

smue@unimelb.edu.au

In Brief

How T cell activation and the delivery of $CD4^+$ T cell help is coordinated in the lymph nodes after infection is poorly understood. Mueller and colleagues demonstrate that $CD4^+$ and $CD8^+$ T cells are activated by different DC subpopulations and with different kinetics after peripheral virus infection.

Hor et al., 2015, Immunity *43*, 554–565
September 15, 2015
http://dx.doi.org/10.1016/j.immuni.2015.07.020

Spatiotemporally Distinct Interactions with Dendritic Cell Subsets Facilitates CD4$^+$ and CD8$^+$ T Cell Activation to Localized Viral Infection

Jyh Liang Hor,[1,2,3] Paul G. Whitney,[1,3] Ali Zaid,[1,2] Andrew G. Brooks,[1,4] William R. Heath,[1,2,4] and Scott N. Mueller[1,2,4,*]
[1]Department of Microbiology and Immunology, The University of Melbourne, at the Peter Doherty Institute for Infection and Immunity, Parkville, VIC 3010, Australia
[2]The Australian Research Council Centre of Excellence in Advanced Molecular Imaging, The University of Melbourne, Parkville, VIC 3010, Australia
[3]Co-first author
[4]Co-senior author
*Correspondence: smue@unimelb.edu.au
http://dx.doi.org/10.1016/j.immuni.2015.07.020

SUMMARY

The dynamics of when and where CD4$^+$ T cells provide help for CD8$^+$ T cell priming and which dendritic cells (DCs) activate CD4$^+$ T cells in vivo after localized infection are poorly understood. By using a cutaneous herpes simplex virus infection model combined with intravital 2-photon imaging of the draining lymph node (LN) to concurrently visualize pathogen-specific CD4$^+$ and CD8$^+$ T cells, we found that early priming of CD4$^+$ T cells involved clustering with migratory skin DCs. CD8$^+$ T cells did not interact with migratory DCs and their activation was delayed, requiring later clustering interactions with LN-resident XCR1$^+$ DCs. CD4$^+$ T cells interacted with these late CD8$^+$ T cell clusters on resident XCR1$^+$ DCs. Together, these data reveal asynchronous T cell activation by distinct DC subsets and highlight the key role of XCR1$^+$ DCs as the central platform for cytotoxic T lymphocyte activation and the delivery of CD4$^+$ T cell help.

INTRODUCTION

The priming of T cell responses to peripheral infections where the pathogen remains localized within the tissues requires the coordination of a variety of immune cells. Dendritic cells (DCs) are necessary to present antigens and provide appropriate costimulatory signals for the efficient activation of T cells. A number of phenotypically and functionally distinct subsets of DCs populate the lymphoid and non-lymphoid tissues and can play unique roles in T cell activation (Heath and Carbone, 2009; Merad et al., 2013). For example, the CD8α^+ DCs, which reside in lymphoid organs, are specialized for the cross-presentation of antigens on major histocompatibility complex (MHC) class I for CD8$^+$ T cell activation (Schnorrer et al., 2006), participate in viral immunity (Belz et al., 2004a, 2005), and belong to an XCR1$^+$, Batf3-dependent lineage that is important for cytotoxic T lymphocyte (CTL)- and T helper 1 (Th1) cell-mediated immunity (Edelson et al., 2010; Hildner et al., 2008). However, these lymph-node-resident DCs rarely act alone, especially during localized infections where they rely upon the activation and migration of tissue-associated DCs to deliver antigens to the lymph node (LN) (Allan et al., 2006; Belz et al., 2004b; Igyártó et al., 2011; Lee et al., 2009). Many vaccines and experimental infection models can, however, bypass a requirement for migratory DCs for T cell priming when injected antigens or pathogens drain directly to the LN via the lymphatic vessels (Gerner et al., 2015; Hickman et al., 2008; Itano et al., 2003; Kastenmüller et al., 2013).

The process of peripheral DC migration to LN can take multiple days, during which time different subsets of DCs emigrate from the tissues to the draining lymph node (dLN). In the skin after herpes simplex virus (HSV) infection, CD11b$^+$ dermal DCs are the first to reach the dLN (Allan et al., 2006), followed by Langerhans cells, whereas CD103$^+$ dermal DCs contribute appreciably to antigen presentation only after secondary spread of the virus across the skin (Bedoui et al., 2009). Some of these skin-migratory DCs are able to transfer antigens to LN-resident DCs, including CD8α^+ DCs, facilitating CD8$^+$ T cell activation (Allan et al., 2006). How this process of antigen handover occurs is not known, although the arrival of infected or antigen-carrying migratory DCs from the peripheral tissues might promote interactions with LN-resident DCs because recent migrants rapidly populate the LN paracortex after entering via the lymphatics (Braun et al., 2011; Kissenpfennig et al., 2005).

The current paradigm of T cell activation predicts that both CD8$^+$ and CD4$^+$ T cells will receive signals from DCs synchronously and become activated and divide with similar kinetics. Yet the involvement of different DC subsets in this process indicates that CD4$^+$ and CD8$^+$ T cells might not interact with DCs at the same time. Although such 3-cell interactions capably describe the existing model, temporally staggered interactions between CD4$^+$ and CD8$^+$ T cells and DCs have also been suggested (Ridge et al., 1998). Indeed, the discovery that multiple DC subsets can stimulate CD4$^+$ T cells ex vivo after HSV infection, whereas CD8$^+$ T cells can respond only to antigens presented by CD8α^+ DCs in the early phase of the response (Allan et al., 2003; Bedoui et al., 2009), raises the possibility that

$CD4^+$ T cells could be primed by a different subset of DCs and subsequently engage the DCs that prime CTLs. Furthermore, a number of infections require $CD4^+$ T cell help via CD40L stimulation for maximal $CD8^+$ T cell responses and memory (Wiesel and Oxenius, 2012), including HSV infection (Smith et al., 2004). Exactly how and when $CD4^+$ T cells provide help to DCs remains poorly understood. $CD4^+$ T cells might be required to provide help to DCs and then recruit naive $CD8^+$ T cells to help DCs for more efficient priming (Castellino et al., 2006). One hypothesis arising from these observations is that $CD4^+$ T cells that become activated early would be more capable of providing help to DCs and thus promoting $CD8^+$ T cell responses.

A number of studies have focused on the initiation of immune responses subsequent to the drainage of lymph-borne antigens, particulates, or pathogens, revealing that subcapsular sinus-lining macrophages and DCs resident in this location can capture antigens (Carrasco and Batista, 2007; Gerner et al., 2015; Hickman et al., 2008; Junt et al., 2007; Phan et al., 2007). These antigen-presenting cells (APCs) can become infected by lymph-borne pathogens and present antigens directly to T cells. Assessment of the spatial and temporal aspects of T cell priming to such lymph-borne antigens have revealed that early $CD8^+$ T cell interactions occur mainly in the peripheral paracortex and interfollicular regions (Gerner et al., 2015; Hickman et al., 2008; Kastenmüller et al., 2013). In contrast, the spatiotemporal dynamics of T cell priming after a localized infection where lymph-borne transport of pathogens is absent has not been examined. To determine the dynamics of $CD4^+$ and $CD8^+$ T cell priming after a localized peripheral virus infection and investigate interactions with DCs, here we have utilized cutaneous infection with HSV-1, a robust model of peripheral infection, combined with intravital 2-photon microscopy. We found that the activation of virus-specific $CD4^+$ and $CD8^+$ T cells, after localized infection, was temporally regulated by interactions with different subsets of DCs. $CD4^+$ T cells interacted with migratory DCs arriving from the infected skin within 14 hr of infection and became activated. Conversely, $CD8^+$ T cells were unable to see migratory APCs and were delayed in their interaction with LN-resident $XCR1^+$ DCs. $CD4^+$ T cells participated in dynamic clusters of $CD8^+$ T cells on $XCR1^+$ DCs that were the critical platform for CTL priming and the delivery of $CD4^+$ T cell help. These findings reveal a previously unidentified level of control of T cell activation to peripheral infection.

RESULTS

Spatiotemporally Distinct Responses by Virus-Specific $CD4^+$ and $CD8^+$ T Cells after Localized Skin HSV Infection

To begin to explore the kinetics of both $CD4^+$ and $CD8^+$ T cell priming after localized infection, we utilized a well-characterized model of cutaneous HSV-1 infection of mice that induces robust $CD4^+$ and $CD8^+$ T cell responses and memory (Gebhardt et al., 2011; van Lint et al., 2004). Prior to infection, animals were adoptively transferred with $CD4^+$ and $CD8^+$ T cells from T cell receptor (TCR) transgenic mice. gDT-II $CD4^+$ T cells specific for an HSV glycoprotein D epitope (Bedoui et al., 2009) and gBT-I $CD8^+$ T cells specific for an HSV glycoprotein B epitope (Mueller et al., 2002a) were backcrossed onto mice ubiquitously expressing the fluorescent proteins GFP or DsRed to allow efficient tracking of small populations of cells by microscopy. Initial priming and expansion of T cells after flank HSV infection occurs in the draining brachial LN followed by emigration to the afferent axillary LN and release into the circulation (Eidsmo et al., 2012). When we examined gDT-II and gBT-I T cell numbers in the brachial LN 3 days after infection, we noted that $CD4^+$ T cells began accumulating sooner than $CD8^+$ T cells (Figure 1A). Both populations of virus-specific T cells peaked in number in the brachial LN 5–6 days after infection. $CD4^+$ T cells then accumulated in the afferent axillary LN 3–4 days after infection, indicating egress from the brachial LN (Figure 1B). In contrast, gBT-I T cells entered the axillary LN only at day 5. In line with these observations, $CD4^+$ T cells first appeared in the spleen at day 4, and $CD8^+$ T cells 1 day later at day 5 (Figure 1C).

To ascertain whether these dissimilar $CD4^+$ and $CD8^+$ T cell response kinetics reflected differences in the location of the cells within the LN, we examined whole LN sections by microscopy. Tissues were co-stained with antibodies against LYVE-1 to detect lymphatics and B220 to visualize B cell follicles (Figure 1D). Both $CD4^+$ and $CD8^+$ T cells localized predominantly to the T cell zone 3 days after infection (Figures 1D and 1F). In contrast, 1 day later the virus-specific $CD4^+$ T cells exhibited reduced accumulation in T cell zones and were observed in the medullary as well as at the subcapsular sinus (SCS) and within B cell follicles (Figures 1D, 1F, and S1). At this time point, the majority of the gBT-I $CD8^+$ T cells remained in the deep T cell zone and interfollicular regions. Concomitant with this, $CD4^+$ T cells were found concentrated in the medullary regions of the axillary LN, indicative of migration from the upstream brachial LN (Figure 1E). By day 5 of infection, $CD8^+$ T cells displayed a similar pattern of intranodal migration, with many gBT-I T cells now observed in the medulla of the brachial LN and afferent axillary LN. This delayed pattern of $CD8^+$ T cell migration was reflected in the systemic diaspora of the cells, whereby $CD4^+$ T cells migrated to the spleen and the infected skin by day 4, yet $CD8^+$ T cells were absent from these sites until day 5 of HSV infection (Figures 1G and 1H). These data indicate that $CD4^+$ T cell responses in the draining LN and subsequent migration to infected peripheral tissues preceded that of the $CD8^+$ T cells, potentially giving the helper T cells a temporal advantage.

Rapid $CD4^+$ T Cell Priming in LN Follows Localized Virus Infection

The previous experiments suggested that $CD4^+$ T cell responses developed more rapidly than $CD8^+$ T cell responses after localized skin HSV infection. To examine whether this corresponded with initial activation and expansion of $CD4^+$ T cells preceding $CD8^+$ T cells, we labeled congenically marked gDT-II and gBT-I T cells with CellTrace Violet prior to adoptive transfer into mice. After skin HSV infection, virus-specific T cells were assessed for upregulation of the early activation marker CD69. Within 12 hr of infection, a proportion of gDT-II $CD4^+$ T cells had upregulated CD69, whereas expression on the gBT-I $CD8^+$ T cells remained undetectable until 24–48 hr after infection (Figures 2A and 2B). $CD4^+$ T cells responding to the infection began dividing within 48 hr, demonstrated by CellTrace Violet dilution in a proportion of cells (Figures 2A and 2C). In contrast, $CD8^+$ T cells showed delayed proliferation beginning 2–3 days after

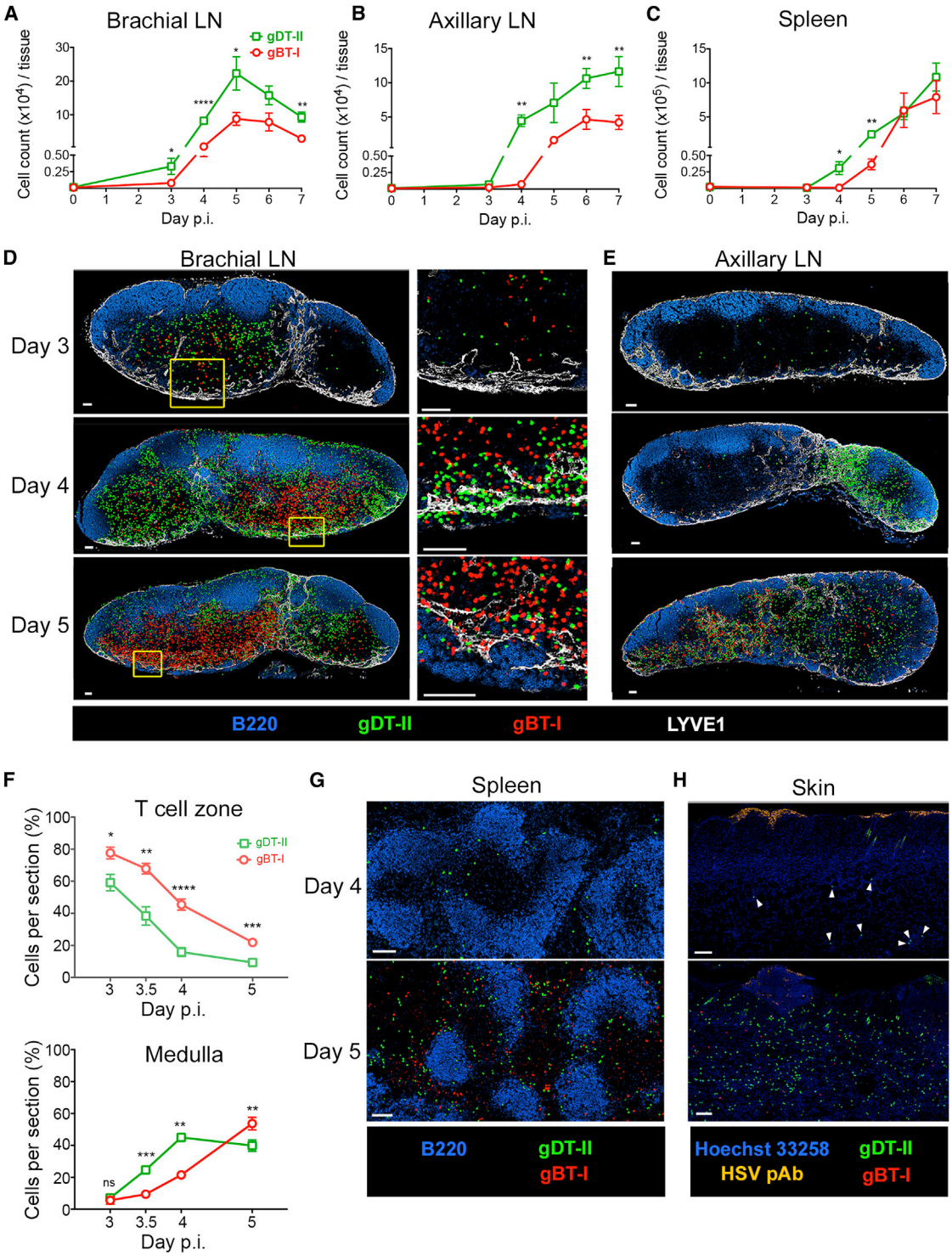

Figure 1. Distinct Kinetics and Spatiotemporal Distribution of CD4⁺ and CD8⁺ T Cells after Cutaneous HSV-1 Infection

gDT-II CD4⁺ and gBT-I CD8⁺ T cells were cotransferred into recipient mice 1 day prior to epicutaneous HSV-1 infection.

(A–C) Total number of gDT-II CD4⁺ (green) and gBT-I CD8⁺ (red) T cells recovered from draining brachial LN (A), downstream axillary LN (B), and the spleen (C) over the course of HSV-1 infection. Data pooled from 2 independent experiments; n = 5–7 mice for each time point.

(D) Confocal images showing spatial distribution of gDT-II CD4⁺ (green) and gBT-I CD8⁺ (red) T cells in draining brachial LNs from days 3–5 p.i.; magnified regions of the medulla are shown in the panels on the right. LYVE-1⁺ lymphatic vessels are stained in white and B220⁺ B cells in blue.

(E) Confocal images showing the infiltration of gDT-II CD4⁺ (green) and gBT-I CD8⁺ (red) T cells into the afferent axillary LNs from days 3–5 p.i.

(legend continued on next page)

infection. This could not be attributed to differential responsiveness of the two transgenic T cell subsets, because both responded after subcutaneous inoculation of titrated doses of peptide, with gBT-I cells displaying slightly greater sensitivity (Figure S2A). When we examined early CD8$^+$ T cell activation in MHC-II-deficient mice where CD4$^+$ T cell responses are absent, a further delay in CD69 upregulation by gBT-I CD8$^+$ T cells was evident (Figure 2D). This showed that asynchronous activation of CD4$^+$ and CD8$^+$ T cells occurred after localized skin HSV infection. We have previously shown that CD4$^+$ T cell help is required for optimal CD8$^+$ T cell priming to HSV infection (Smith et al., 2004). These data further suggest that CD4$^+$ T cell help is required to promote rapid CTL priming.

CD4$^+$ T Cells Cluster in LN Early after Infection

We next sought to examine the dynamics of these early T cell priming events after HSV infection. To do this, we employed a modified flank HSV infection model that resulted in priming of the T cell responses in the draining inguinal LN. The kinetics of CD4$^+$ and CD8$^+$ T cell activation, proliferation, and migration was the same using this method compared to the standard site of flank infection (Figures S2B–S2D). We then utilized intravital 2-photon microscopy to visualize the behavior of responding gDT-II and gBT-I T cells in the draining LN early after infection. Within 12 hr of infection, we observed marked clustering of the gDT-II CD4$^+$ T cells in the T cell zone that displayed a significantly reduced average velocity in comparison to T cells migrating in LN of naive uninfected mice (Figures 3A–3C, Movie S1). Most notably, gBT-I CD8$^+$ T cells in the immediate vicinity of CD4$^+$ T cell clusters showed no obvious change in motility or behavior. The CD8$^+$ T cells did not cluster in the LN at this early time point, suggesting that they were ignorant of the APC driving CD4$^+$ T cell activation. In accordance with the temporal proliferation data shown in Figure 2, these data indicated that DCs presenting antigen (Ag) on MHC-I were not yet present or accessible to the CD8$^+$ T cells at this early stage.

When we examined CD4$^+$ and CD8$^+$ T cell behavior 40–48 hr after infection, we observed that both T cell subsets now formed dynamic clusters (Figures 3A and 3B, Movie S2). Both populations of cells displayed a reduced overall migrational velocity and greater mean confinement and a substantial proportion of each cell type participated in clusters within each imaging volume (Figures 3C–3E and S2E). We noted that many of the clusters contained mostly CD4$^+$ or CD8$^+$ T cells as opposed to relatively equal proportions of both cell types. Conspicuously, we also observed transient interactions between migrating CD4$^+$ T cells that visited CD8$^+$ T cells clusters. Clustering of the T cells was antigen specific—no clustering was observed among non-specific OT-II and OT-I T cells present in the LN at the same time (Figures 3F–3H and S2F, Movie S3). We did find that the OT-II CD4$^+$ T cells showed a slightly reduced average velocity in the LN of HSV-infected mice. This indicated that the microenvironment of the inflamed LN also influenced T cell migration.

To enumerate T cell clustering in the LN, and because intravital 2-photon microscopy is restricted to the first few hundred microns of the tissue (preventing imaging of the deep paracortex), we imaged thick whole LN sections and quantitated CD4$^+$ and CD8$^+$ T cell clusters. As expected from our intravital movies, we observed extensive clustering of gDT-II T cells 18 hr after infection, with approximately 20% of the CD4$^+$ T cells involved in clusters throughout the LN paracortex, whereas gBT-I T cells did not cluster (Figures 4A, 4B, and 4E). Similar numbers of gDT-II and gBT-I clusters were found 42 hr after infection (Figures 4C–4E). Given the dynamic nature of the clusters we observed by intravital 2-photon microscopy, whereby some cells were seen entering and exiting clusters, this static analysis of cluster frequency might reflect an underestimate of the true proportion of cells involved in clusters. When we assessed the composition of the clusters, we found that a substantial proportion was composed of only CD4$^+$ or CD8$^+$ T cells (Figure 4F). This supported our intravital imaging data, raising the possibility that the homogenous clusters of T cells were interacting with different DCs. Consistent with differential DC subset presentation, we also noted that CD8$^+$ T cells formed clusters in more localized regions of the LN paracortex in all mice examined, as opposed to CD4$^+$ T cells clusters that were distributed across one or both lobes of the draining LN (Figure 4D).

Migratory DCs Activate CD4$^+$ T Cells Early after Infection

The above data suggested that the temporally and spatially segregated clusters of CD4$^+$ and CD8$^+$ T cells might be interacting with different APCs specializing in presentation of antigens on MHC class I or II. Although we observed predominantly CD4$^+$ T cells clustering in the early phase of the response (12–24 hr), very rare CD8$^+$ T cell clusters were observed in some of the mice (one to two clusters in two mice out of eight). Recent studies have shown that priming of CD8$^+$ T cell responses to lymph-borne virus infection involves clustering of CD8$^+$ T cells with infected cells (Hickman et al., 2011; Kastenmüller et al., 2013). We could not detect drainage of fluorescently labeled HSV from the site of infection on the flank to the draining LN after infection (Figures S3A and S3B). We were also unable to detect any virus in the LN within the first 3 days of HSV flank infection by microscopy or plaque assay. In contrast, after footpad inoculation, lymph-borne virus rapidly entered the draining LN and localized to the SCS where we could distinguish infected cells, including CD169$^+$ SCS macrophages (Figure S3C). We observed CD8$^+$ T cell clusters around virus-infected cells in the interfollicular regions and outer paracortex (cortical ridge) after lymph-borne infection (Figure S3D). Thus, CD8$^+$ T cells clustered early with infected cells when virus drained to the LN. Moreover, proliferation of the CD4$^+$ and CD8$^+$ T cells proceeded synchronously after lymph-borne infection (Figures S3E and S3F). Taken together, this suggests that there was no significant contribution to T cell priming by directly infected cells in the LN after localized skin HSV infection, the focus of our studies.

(F) Proportion of gDT-II CD4$^+$ (green) and gBT-I CD8$^+$ (red) T cells occupying the T cell zone (top) and medulla (bottom) of the draining brachial LN from days 3–5 p.i., quantitated per LN section. Data pooled from 2 independent experiments; n = 5–6 mice per time point. See also Figure S1.
(G and H) Confocal images of the spleen (G) and infected skin (H) from days 4–5 p.i.
All scale bars denote 100 μm. Error bars represent mean ± SEM. *$p < 0.05$; **$p < 0.01$; ***$p < 0.001$; ****$p < 0.0001$; ns, not significant.

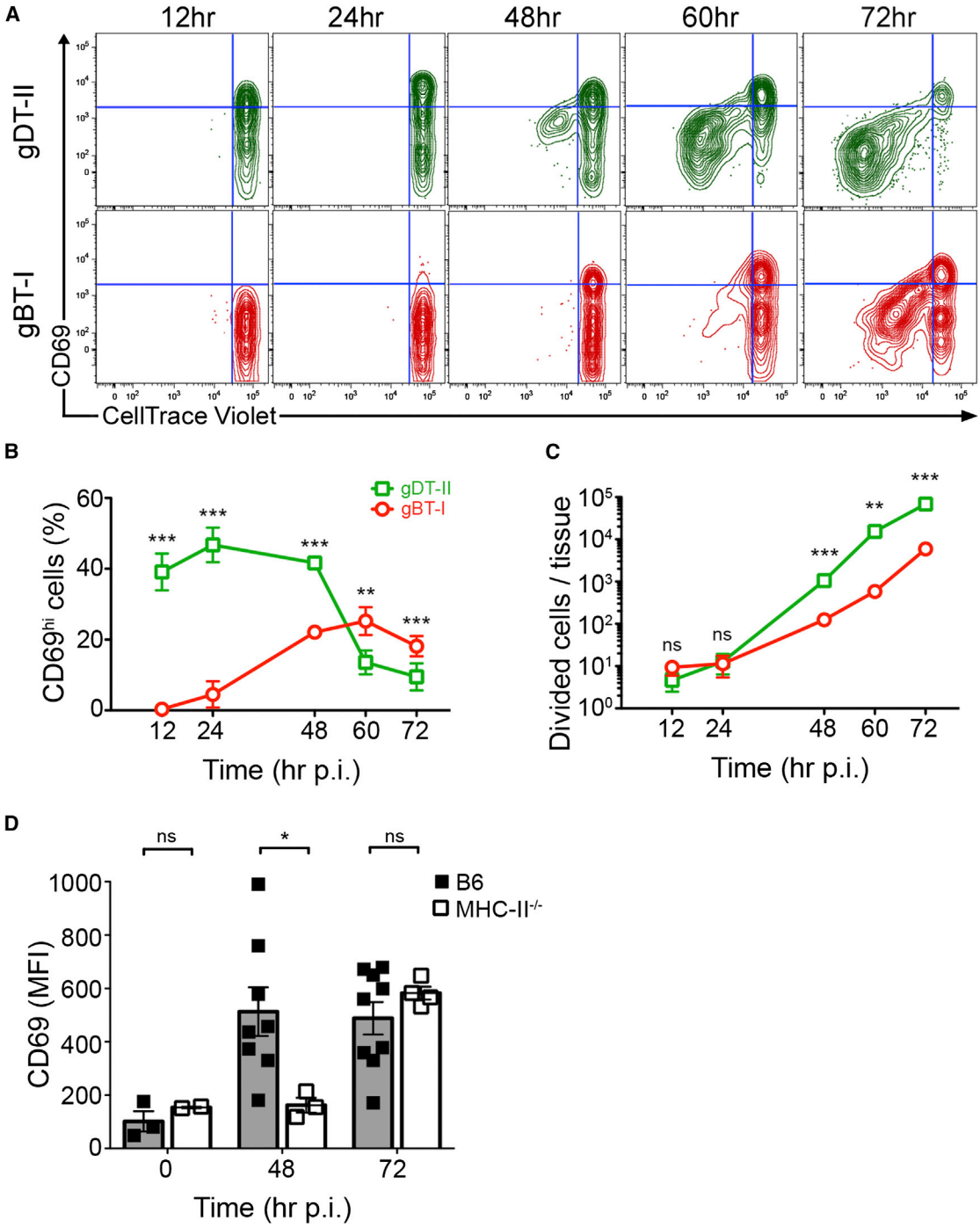

Figure 2. Differential Priming Kinetics of CD4$^+$ and CD8$^+$ T Cells after Cutaneous HSV-1 Infection

CellTrace Violet-labeled gDT-II CD4$^+$ and gBT-I CD8$^+$ T cells were adoptively transferred into recipient mice 1 day prior to epicutaneous HSV-1 infection.

(A) Upregulation of the early activation marker CD69 by gDT-II CD4$^+$ (top, green) and gBT-I CD8$^+$ (bottom, red) T cells in draining brachial LN from 12 to 72 hr p.i.

(B) Proportion of CD69^{hi} gDT-II CD4$^+$ and gBT-I CD8$^+$ T cells in draining brachial LN over 72 hr p.i.

(C) Number of divided cells (CellTrace Violet$_{lo}$) recovered per draining brachial LN over 72 hr p.i.

(D) Mean fluorescence intensity of gBT-I CD8$^+$ T cells in draining brachial LN of B6 and MHC-II$^{-/-}$ mice at various time points after infection.

Data in (A)–(C) pooled from 2–3 independent experiments; n = 6–12 mice per time point. Error bars represent mean ± SEM. *p < 0.05; **p < 0.01; ***p < 0.001; ns, not significant. See also Figure S2.

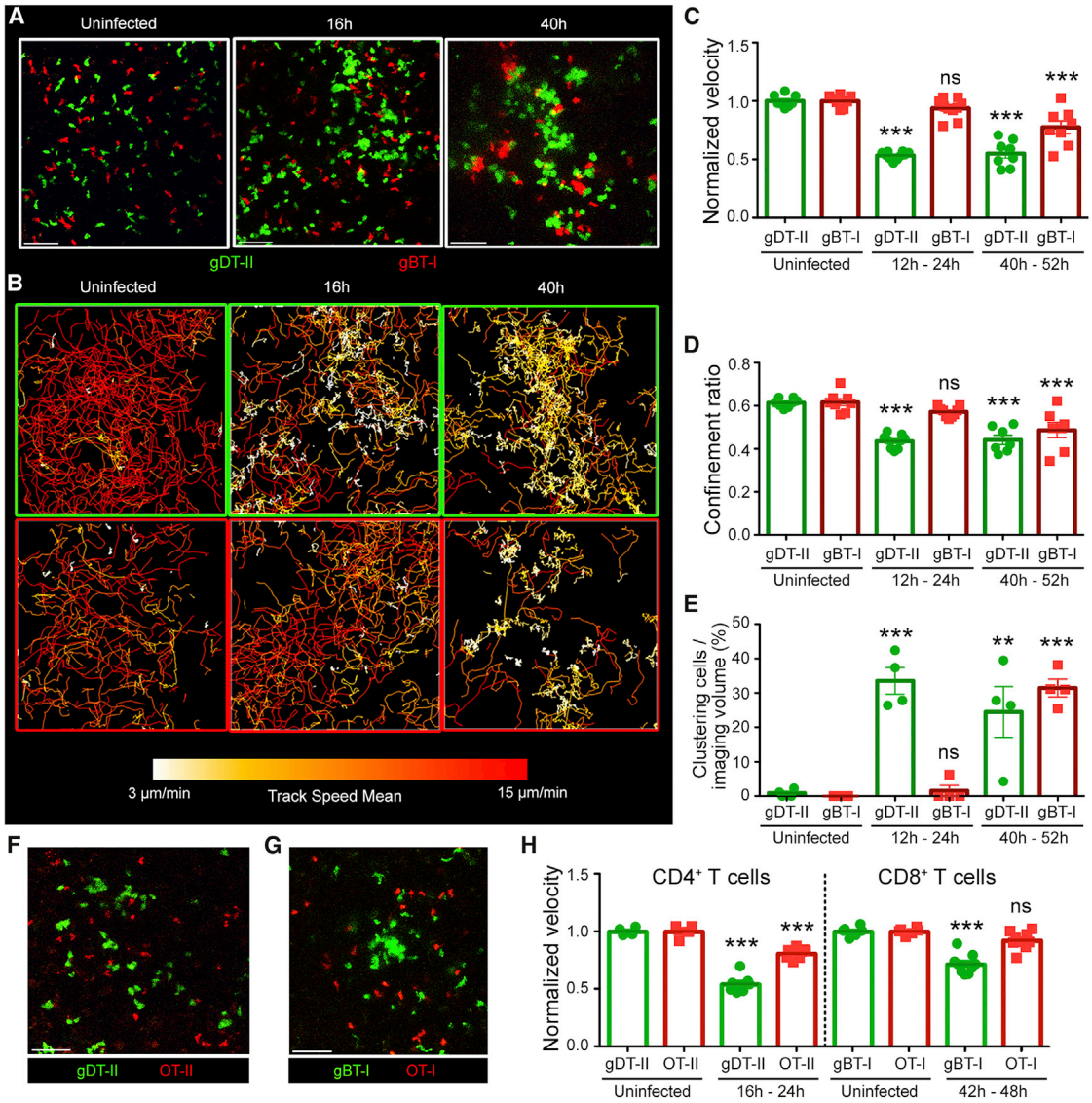

Figure 3. Early Clustering of HSV-Specific CD4$^+$ T Cells in Draining LN

gDT-II.EGFP CD4$^+$ and gBT-I.DsRed CD8$^+$ T cells were adoptively transferred into recipient mice prior to epicutaneous HSV-1 infection.

(A) Maximum intensity projection images showing clustering of gDT-II CD4$^+$ (green) and gBT-I CD8$^+$ (red) T cells in the T cell zone on the inguinal LN (imaging depth ~150–200 µm under LN capsule) at different phases of infection: uninfected (left), early (16 hr, middle), and late (40 hr, right). See also Movies S1 and S2.

(B) Cell tracks of gDT-II CD4$^+$ (top) and gBT-I CD8$^+$ (bottom) color coded to display mean track velocity at the indicated time points. Red tracks correspond to higher track velocities and white tracks show slower cell tracks. Data from Movies S1 and S2.

(C and D) Mean velocity (C) and mean confinement ratio (D) of cell tracks normalized to naive cells. Each data point represents the mean velocity (C) or confinement ratio (D) of all cell tracks per movie. Data pooled from at least two independent experiments; n = 2–4 movies each from 2–6 mice per time point.

(E) Proportion of clustering cells in the LN after infection. Each data point represents the proportion of clustering gDT-II CD4$^+$ and gBT-I CD8$^+$ T cells in each imaging volume. Data pooled from 2 independent experiments; n = 4 mice per time point.

(F and G) Maximum intensity projection images showing a snapshot of the behavior of (F) gDT-II and OT-II CD4$^+$ T cells and (G) gBT-I and OT-I CD8$^+$ T cells after infection. See also Movie S3.

(H) Mean velocity of cell tracks normalized to migration in uninfected mice. Each data point represents the mean velocity of all cell tracks per movie. Data pooled from 2 independent experiments; n = 1–2 movies each from 4–7 mice.

Error bars represent mean ± SEM. *p < 0.05; **p < 0.01; ***p < 0.001; ns, not significant. See also Figure S2.

The preceding experiments showed that temporally segregated antigen presentation occurred after flank HSV infection. Prior studies have shown that migratory subsets of DCs are essential for CD8$^+$ T cell responses after skin HSV infection (Allan et al., 2006; Stock et al., 2004). To examine whether migratory APCs were involved in the priming of the CD4$^+$ T cell response in vivo after localized HSV infection, we painted the flank skin of mice with the fluorescent dye TRITC prior to virus inoculation. This enabled tracking and visualization of DCs migrating from the skin to the draining LN (Figure S4). Migratory TRITC$^+$ APCs

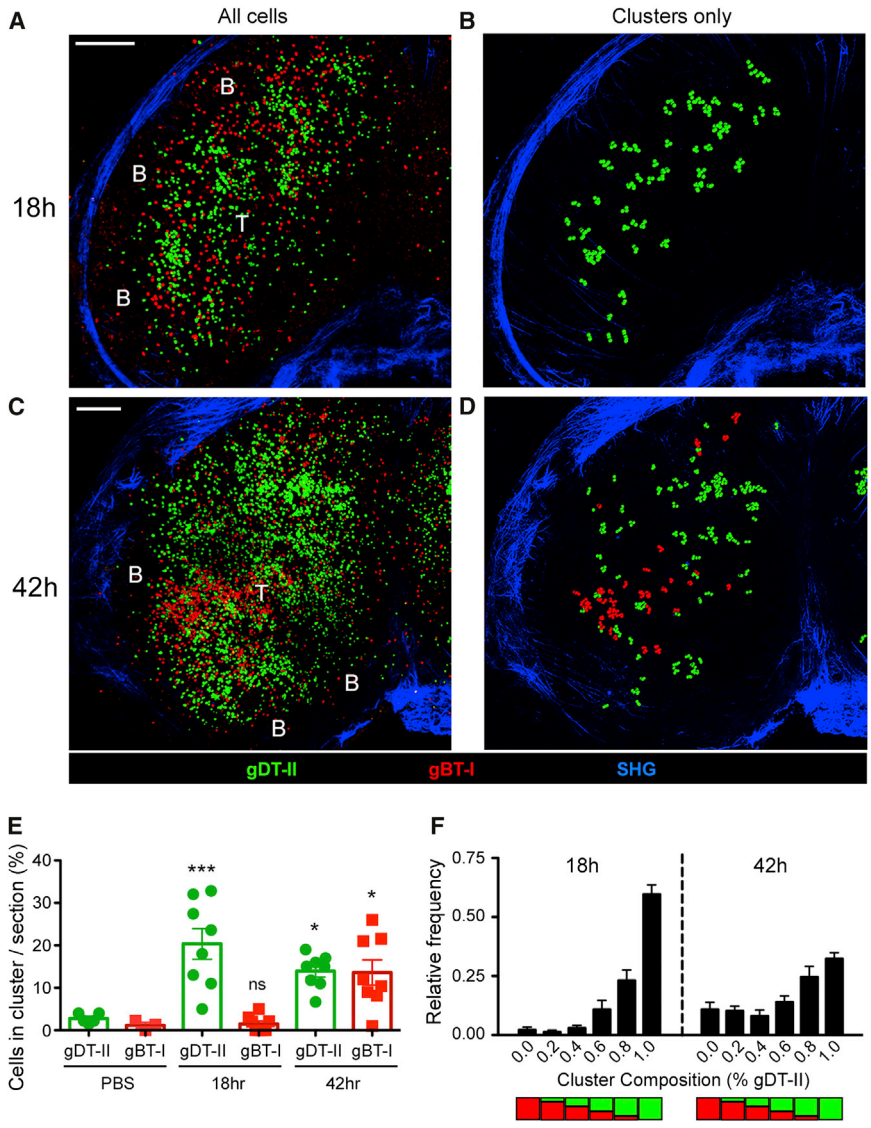

Figure 4. Spatial and Temporal Distribution of T Cell Clusters after Cutaneous HSV-1 Infection

gDT-II.EGFP CD4$^+$ and gBT-I.DsRed CD8$^+$ T cells were adoptively transferred into recipient mice 1 day prior to epicutaneous HSV-1 infection.

(A and C) Maximum intensity projection images of thick inguinal LN sections (imaging volume 100–120 μm thickness) showing the distribution of gDT-II CD4$^+$ (green) and gBT-I CD8$^+$ (red) cells during early (A) and late (B) phase of infection.

(B and D) Location of clustering cells in ILN sections corresponding to (A) and (C), represented in green (gDT-II CD4$^+$) or red (gBT-I CD8$^+$) spots.

(E) Percentage of clustering cells per LN section.

(F) Composition of each cluster comprised of a minimum of four cells. A value of 1.0 represents homogenous (100%) gDT-II CD4$^+$ T cell clusters and 0.0 represents 100% gBT-I CD8$^+$ T cell clusters.

Error bars represent mean ± SEM. $^{**}p < 0.01$; $^{***}p < 0.001$; ns, not significant. Data pooled from 2 independent experiments; n = 4–8 mice per time point. See also Figure S3.

entered the LN via the SCS and accumulated in the paracortex by 18 hr. By 40 hr after infection, the majority of the TRITC$^+$ cells had migrated through the paracortex and were concentrated closer to medullary regions, similar to the path of intralymphatically injected DCs observed migrating through LN (Braun et al., 2011).

Clusters of gDT-II CD4$^+$ T cells and TRITC$^+$ cells formed early after infection (Figure 5A). Later in the response (40–48 hr), when both CD4$^+$ and CD8$^+$ T cell clusters were established, few clusters were directly associated with TRITC$^+$ migratory APCs. These data indicated that early activation of CD4$^+$ T cells, but not CD8$^+$ T cells, probably involved interactions with migratory DCs. To test this hypothesis, we co-stained thick sections of LN tissue with antibodies against CD69 to visualize where the recently activated T cells localized. In the early phase of the response, CD69 was upregulated on gDT-II CD4$^+$ T cells clustering around TRITC$^+$ APCs (Figure 5B). At this time (20 hr), gBT-I CD8$^+$ T cells remained CD69 negative. When we examined LNs a day later, CD69 was upregulated on CD8$^+$ T cells, but these cells were not clustering with TRITC$^+$ cells.

We next examined the dynamics of the virus-specific T cell interactions with the TRITC$^+$ migratory APCs in the LN via intravital 2-photon microscopy. The gDT-II CD4$^+$ T cells swarmed around a subset of TRITC$^+$ migratory APCs (Figure 5C, Movies S4 and S5). CD4$^+$ T cells participating in these dynamic clusters with TRITC$^+$ APCs demonstrated both transient and stable interactions, with many cells remaining in contact with APC for >30 min (Figures 5D and 5E). As anticipated, CD8$^+$ T cells engaged only transiently with the TRITC$^+$ DCs and did not slow down, similar to that after mock infection with PBS (Figures 5C–5E, Movies S4 and S5). Together, these data reveal that CD4$^+$ T cells were being activated by migratory APCs after localized skin HSV infection. In contrast, CD8$^+$ T cells did not interact with migratory DCs and remained naive during the early phase of the response in the absence of direct virus drainage.

XCR1$^+$ LN-Resident DCs Are Required for CD8$^+$ T Cell Priming and CD4$^+$ T Cell Help

Migratory APCs are necessary for CD8$^+$ T cell priming after skin HSV infection (Allan et al., 2006; Stock et al., 2004). We hypothesized that migrants could present skin-acquired, virion-derived antigens on MHC-II, yet were unable to cross-present viral antigens to CD8$^+$ T cells. In a prior study we found that antigen presentation for the immunodominant gBT-I epitope ($gB_{498-505}$) required de novo synthesis, yet expression was rapid and was detectable by CTL within 2 hr of infection (Mueller et al., 2003). When we infected mice on the skin with UV-inactivated HSV (UV-HSV), only gDT-II T cells were activated (Figure S5),

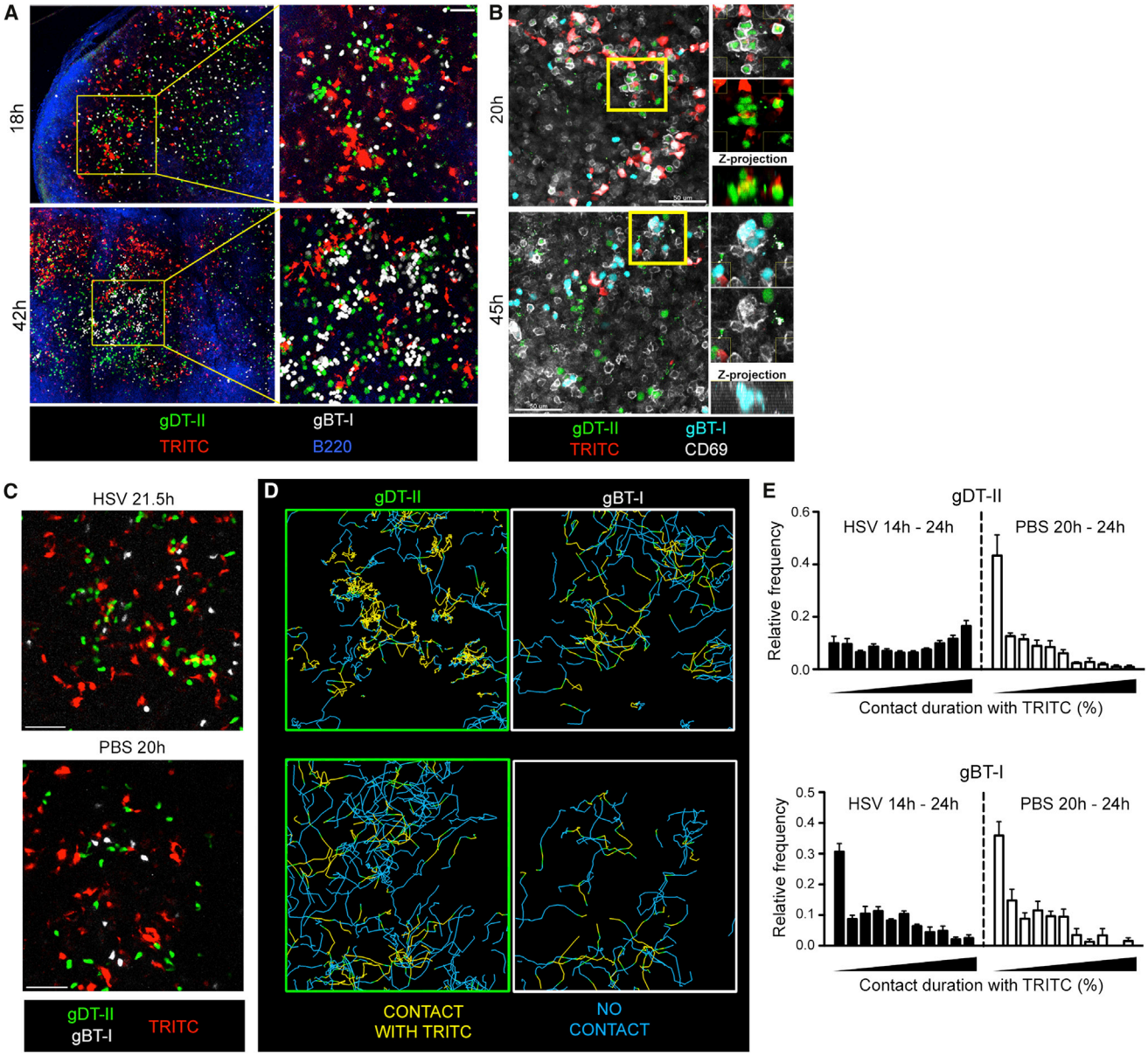

Figure 5. HSV-Specific CD4$^+$ T Cells Preferentially Interact with Migratory APCs during Early HSV-1 Infection

(A) Maximum intensity projection images of thick inguinal LN sections showing the localization of TRITC$^+$ cells (red), gDT-II CD4$^+$ (green), and gBT-I CD8$^+$ (white) T cells at early (top) and late (bottom) phases of infection. Scale bars represent 100 μm.

(B) Maximum intensity projection images of thick inguinal LN sections showing anti-CD69 staining (white), gDT-II (green), gBT-I (cyan), and TRITC (red). Scale bars represent 50 μm.

(C) Maximum intensity projection images from time-lapse movies showing interactions between gDT-II CD4$^+$ (green) and gBT-I CD8$^+$ (white) T cells with TRITC-painted cells (red) in early infected (top) or mock infected (bottom) mice. Scale bars represent 50 μm. See also Movie S4.

(D) Cell tracks color-coded to show contact (yellow) or no contact (light blue) with TRITC$^+$ DCs. gDT-II CD4$^+$ (green box) and gBT-I CD8$^+$ (white box) tracks correspond to Movie S4. See also Movie S5.

(E) Contact duration with TRITC$^+$ cells by gDT-II CD4$^+$ (left) and gBT-I CD8$^+$ (right) T cells in early infected (black bars) and mock infected (white bars) mice. Data pooled from 1–2 independent experiments; n = 4–9 mice per time point. See also Figure S4. Error bars represent mean ± SEM.

further supporting a requirement for de novo synthesis of gB for MHC-I presentation while demonstrating that virion-derived antigen could be presented on MHC-II. Thus, skin migratory CD11b$^+$ DCs were unable to cross-present antigens on MHC-I and/or the availability of gB for cross-presentation was insufficient prior to viral protein synthesis.

The above data demonstrated that CD4$^+$ T cells were activated by migratory DCs, yet we had previously shown that the LN-resident CD8α^+ DCs are the only cells capable of stimulating CD8$^+$ T cells ex vivo after HSV infection (Bedoui et al., 2009). We next examined the T cell-DC interactions driving CD8$^+$ T cell clustering and activation by 2-photon microscopy in *Itgax*-EYFP mice

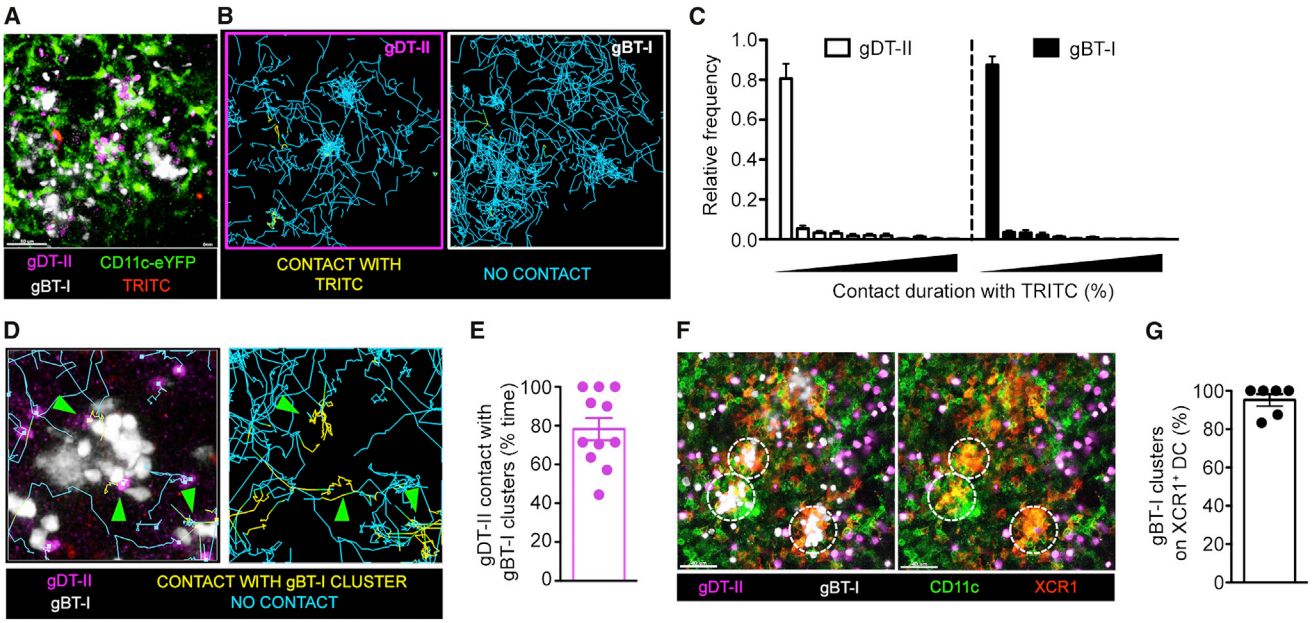

Figure 6. CD8$^+$ T Cell Priming by XCR1$^+$ LN-Resident DCs

(A) Maximum intensity projection images from time-lapse movies of ILN in HSV-infected *Itgax*-EYFP mice showing distinct clustering of gBT-I CD8$^+$ T cells (white) with non-migratory DCs (green). Scale bars represent 50 μm. See also Movie S6.

(B) Cell tracks color-coded to show contact (yellow) or no contact (light blue) with TRITC$^+$ DCs. Tracks of gDT-II CD4$^+$ (left) and gBT-I CD8$^+$ (right) correspond to Movie S6.

(C) Duration of contact between gDT-II CD4$^+$ and gBT-I CD8$^+$ T cells with TRITC$^+$ cells. Data pooled from 2 independent experiments, n = 5–6 mice per group. Error bars represent mean ± SEM.

(D) 2P image of inguinal LN showing gDT-II CD4$^+$ T cells (purple) interacting with gBT-I CD8$^+$ T cell clusters (white). Cell tracks color-coded to show contact with gBT-I clusters (yellow) and non-contact (blue) are depicted with a history of 20 frames. Full cell tracks are shown on the right panel. Green arrows denote CD4$^+$ T cells in contact with gBT-I clusters. See also Movie S7.

(E) Proportion of time gDT-II CD4$^+$ T cells were in contact with gBT-I CD8$^+$ T cell clusters per movie. Only CD4$^+$ T cells establishing contact for >5 min with gBT-I clusters were analyzed. Data from one representative experiment of two are shown.

(F) Maximum intensity projection images of thick inguinal LN sections showing localization of gBT-I CD8$^+$ T cell clusters (white) relative to XCR1$^+$ (red) CD11c$^+$ (green) DCs. Dotted circles denote gBT-I clusters. Right panel shows image without gBT-I CD8$^+$ T cells. Scale bars represent 40 μm.

(G) Fraction of gBT-I CD8$^+$ T cell clusters closely associated with XCR1$^+$CD11c$^+$ DCs per mouse. Data pooled from 2 independent experiments; n = 6 mice. See also Figure S5. Error bars represent mean ± SEM.

(commonly known as CD11c-EYFP) to visualize both recent skin migrants (TRITC$^+$CD11c$^+$) and LN-resident DCs (TRITC$^-$CD11c$^+$). The gBT-I T cells clustered on TRITC$^-$ cells in the draining LN 40–48 hr after HSV infection (Figure 6A and Movie S6). These DCs expressed less CD11c, indicative of mature DCs, which upregulate MHC-II and downregulate CD11c upon activation (Singh-Jasuja et al., 2013). Both gBT-I and gDT-II T cells interacted only minimally with TRITC$^+$ migrants at this phase of the response (Figure 6C). Notably, the clusters of CD8$^+$ T cells around CD11c$^+$ DCs were frequently visited by CD4$^+$ T cells that interacted with CD8$^+$ T cells for substantial periods (Figures 6D and 6E and Movie S7). Thus, after activation by migratory DCs, CD4$^+$ T cells access CD8$^+$ T cell clusters on resident DCs, potentially to provide DC-licensing signals involved in CD8$^+$ T cell priming.

We assessed the identity of the DCs involved in CD8$^+$ T cell clustering. Because CD8α^+ DCs are also defined by specific expression of the chemokine receptor XCR1 (Crozat et al., 2011; Dorner et al., 2009), we co-stained LN tissues with antibodies against XCR1 and CD11c. The clusters of CD8$^+$ T cells in LN 42 hr after HSV infection occurred almost exclusively on XCR1$^+$ DCs (Figures 6F and 6G). Thus, although migratory DCs first prime CD4$^+$ T cells after localized HSV infection, CD8$^+$ T cell activation is delayed until resident CD8α^+XCR1$^+$ DCs acquire the capacity to stimulate CTLs. Such temporally separated priming of CD4$^+$ T cells by DCs specialized in MHC-II presentation prior to providing help for CD8$^+$ T cell responses highlights the key role played by XCR1$^+$ DCs in CD8$^+$ T cell activation and the provision of help.

DISCUSSION

The interactions between T cells and DCs and the requirements for T cell activation are increasingly being revealed through intravital imaging. Nevertheless, how both CD4$^+$ and CD8$^+$ T cell responses are initiated after infection and the involvement of different DC subsets in the coordination of T cell priming remains uncertain. To explore this, we utilized peripheral infection with HSV-1, a virus that remains localized within the tissues and requires antigen transport by migratory skin DCs to prime T cell responses in the LN. We found that activation of CD4$^+$ and CD8$^+$ T cells was temporally separated and involved antigen presentation by different subsets of DCs. CD4$^+$ T cells clustered on

migratory DCs that arrived in the draining LN within 9 hr of infection, resulting in their activation. In contrast, $CD8^+$ T cells needed to wait for $XCR1^+$ LN-resident DCs to cross-present antigens and facilitate T cell clustering and activation. $CD4^+$ T cells also interacted with late $CD8^+$ T cell-$XCR1^+$ DC clusters, defining these DCs as a critical platform for the delivery of $CD4^+$ T cell help to $CD8^+$ T cells.

These findings provide insight into the complex interactions involved in the priming of T cell responses to peripheral infection. Rapid activation of $CD4^+$ T cells might enable these cells to provide help via the licensing of DCs. Although it is well established that $CD4^+$ T cell help is required for maximal $CD8^+$ T cell responses to infections including HSV, as well as for fully functional memory T cell populations, the mechanics of this process have not been determined. When and where this occurs, whether $CD4^+$ T cells are activated by the same DCs through which they provide help, or through other DCs, are all questions that need answering. The provision of help requires that $CD4^+$ T cells and $CD8^+$ T cells interact with the same DCs, though whether this process involves simultaneous interactions by $CD4^+$ and $CD8^+$ T cells with DCs or sequential interactions is also not known. Moreover, in order to provide help, $CD4^+$ T cells must first be activated and upregulate CD40L, implicating delayed kinetics of help for CTLs until the $CD4^+$ T cells are activated and capable of licensing DCs.

Here we have provided substantial insight into these dynamic events and demonstrate that migratory DCs activated $CD4^+$ T cells prior to the initiation of $CD8^+$ T cell clustering on $XCR1^+$ DCs. $CD4^+$ T cells then interacted in a dynamic fashion with clusters of $CD8^+$ T cells being stimulated by LN-resident DCs. These studies raise the possibility that pre-activated $CD4^+$ T cells license $CD8\alpha^+XCR1^+$ DCs during $CD8^+$ T cell engagement, which differs for the model where $CD4^+$ T cells attract naive $CD8^+$ T cells to licensed DCs (Castellino et al., 2006). However, we also observed some clusters of $CD4^+$ T cells on LN-resident DCs that did not involve $CD8^+$ T cell clustering, suggesting that licensing of some DCs by $CD4^+$ T cells could also occur prior to $CD8^+$ T cell engagement. Importantly, our observations suggest that such $CD4^+$-DC helper interactions are dynamic and short lived. Although we introduced a higher frequency of naive T cells to image these interactions, at lower precursor frequencies efficient licensing of multiple DCs by rare antigen-specific $CD4^+$ T cells might necessitate that early-activated helper cells move rapidly between APCs for CTL priming.

The exact contribution of different DC subsets to $CD4^+$ T cell priming is not known. Multiple migratory and lymphoid tissue-resident DC subsets have been shown to have the capacity to present antigen to $CD4^+$ T cells ex vivo (Bedoui et al., 2009; Heath and Carbone, 2009; Kim and Braciale, 2009; Lee et al., 2009; Zhao et al., 2003). In our model, the migratory subset involved in antigen presentation early in the response is primarily the $CD11b^+$ dermal DCs, whereas the skin $CD103^+$ DC subset does not contribute until later in the response after secondary viral spread (Bedoui et al., 2009). Here we have shown that migratory DCs played a key role in activating $CD4^+$ T cells, yet were unable to stimulate $CD8^+$ T cell in vivo. Whether early $CD4^+$ T cell activation by migratory DCs is sufficient for optimal effector cell generation or whether signals from $XCR1^+$ DCs are also required for complete maturation and the generation of a robust memory population will be important to determine.

The early activation of $CD4^+$ T cells precipitated rapid intranodal reorganization to B cell follicles and medullary regions, egress to downstream lymph nodes, and more rapid accumulation at the site of infection. These data might help explain how $CD4^+$ T cells facilitate recruitment of $CD8^+$ T cells in the LN to the infected tissues early after infection (Kumamoto et al., 2011; Nakanishi et al., 2009). Though whether such a temporal difference occurs in other infections remains unclear given that we have shown here that lymph-borne infection after subcutaneous injection of virus resulted in synchronous kinetics of $CD4^+$ and $CD8^+$ T cell activation. The epicutaneous HSV-1 infection model used here represents a highly localized peripheral infection that primes robust T cell responses and memory formation. In contrast to beads applied to scarified skin (Gerner et al., 2015), we did not find detectable HSV infection in the LN after localized infection, only after subcutaneous inoculation. We found that the early events in T cell priming to localized infection differed slightly from that after lymph-borne spread of virus, the latter of which resulted in early activation of $CD8^+$ T cells after clustering with infected cells. HSV binds efficiently to receptors in the skin and is restricted by the basement membrane and thus does not drain efficiently to LN (Mueller et al., 2002b; Weeks et al., 2000; Zhao et al., 2003). Infection of DCs in the LN has been shown to be negligible after skin HSV infection (Allan et al., 2006). Although we can't completely exclude that a small number of DCs in the LN are infected, our data suggest that cross presentation is the predominant pathway involved in priming the $CD8^+$ T cell response via $XCR1^+$ DCs.

Taken together, we have identified temporally staggered interactions with different DCs for the priming of $CD4^+$ and $CD8^+$ T cell responses to a localized virus infection. Our data suggest a model whereby migratory DCs transport antigens from the skin to the draining LN and activate $CD4^+$ T cells. Yet, migratory skin DCs are unable to stimulate $CD8^+$ T cells, which require antigen to be delivered to $XCR1^+$ LN-resident DCs for cross-presentation. Crucially, $CD8^+$ T cell clustering with LN-resident DCs involved concurrent interactions with $CD4^+$ T cells, emphasizing the central role that $XCR1^+$ DCs play in orchestrating both CTL priming and the delivery of help during localized infection.

EXPERIMENTAL PROCEDURES

Mice and Infections

C57BL/6, gBT-I (Mueller et al., 2002a), gBT-I.xB6.SJL-PtprcaPep3b/BoyJ (gBT-I.CD45.1), gBT-I.uGFP, gBT-I.dsRed, gDT-II (Bedoui et al., 2009), gDT-II.uGFP, gDT-II x B6.CD45.1, OT-I.uGFP, OT-II.dsRed, *Itgax*-EYFP, and MHC-II deficient (AB°) mice were bred in the Department of Microbiology and Immunology, The University of Melbourne. gBT-I and gDT-II encode transgenes expressing T cell receptor recognizing the HSV-1 glycoprotein B-derived epitope $gB_{498\text{-}505}$ and glycoprotein D-derived epitope $gD_{315\text{-}327}$, respectively. Animal experiments were approved by The University of Melbourne Animal Ethics Committee. Epicutaneous and subcutaneous infections with HSV-1 (KOS strain) were performed as described elsewhere (van Lint et al., 2004; Coles et al., 2002). For imaging experiments, scarification was performed at the hind flank, near the transition of torso-hind limb region to allow drainage to inguinal LN. See also Supplemental Experimental Procedures.

T Cell Enrichment, Labeling, and Adoptive Transfer

T cells were enriched from naive lymph nodes and/or spleens of female transgenic mice through negative enrichment of $CD4^+$ or $CD8^+$ T cells, for gDT-II and gBT-I, respectively. For gDT-II cells, further positive magnetic enrichment was performed as described elsewhere (Bedoui et al., 2009). See also Supplemental Experimental Procedures.

TRITC Painting

Tetramethylrhodamine-5-isothiocyanate (TRITC; Life Technologies) was dissolved in DMSO and diluted to 0.5% (v/v) in acetone. The TRITC solution was painted on a 1 cm^2 diameter region of skin in a 10 μl volume on the depilated flank of anesthetized mice and allowed to dry. Mice were infected with HSV 4–6 hr after TRITC application.

Cell Isolation and Flow Cytometry

Single-cell suspensions were resuspended in PBS containing FCS (2%) and EDTA (5 mM) for antibody staining. For DC isolation, lymph nodes were disrupted with scalpel blade and incubated in 1 mg/ml collagenase type III (Worthington) and 20 μg/ml DNase medium for 20 min before addition of 0.1 M EDTA. Cells were then filtered and resuspended as above for antibody staining. Propidium iodide was added to the samples prior to acquisition by flow cytometry (BD FACS Canto or BD Fortessa). Data were analyzed with FlowJo software (TreeStar). See also Supplemental Experimental Procedures.

Immunofluorescence and Confocal Microscopy

Lymph nodes and spleens were harvested and fixed in PLP fixative for 6–8 hr, washed in PBS twice for 10 min, and incubated in 20% sucrose overnight at 4°C. Tissue sections were cut at 12 μm thickness with a cryostat (Leica CM3050S) and air-dried before being fixed in acetone for 5 min, dried, and then blocked for 20 min (Protein Block X0909, DAKO) at RT. Sections were then stained with primary antibodies for 1.5 hr, washed in PBS for 10 min, and stained with secondary antibodies for 30 min. Images were acquired with an LSM700 or LSM710 confocal microscope (Carl Zeiss) and processed with Imaris (Bitplane), ImageJ (NIH), and Photoshop (Adobe). Determination of the LN compartments was performed with masks for different regions that were generated semi-automatically with ImageJ (NIH) based on anti-B220 and anti-LYVE1 staining. See also Supplemental Experimental Procedures.

Intravital Two-Photon Microscopy

Surgically exposed left inguinal LNs were prepared for intravital imaging via a modified version of a published protocol (Miller et al., 2003; Qi et al., 2006), using an upright LSM710 NLO multiphoton microscope (Carl Zeiss) with a 20×/1.0 NA water immersion objective enclosed in an environmental chamber maintained at 35°C with heated air. Fluorescence excitation was provided by a Chameleon Vision II Ti:sapphire laser (Coherent) with dispersion correction and fluorescence emission detected using external non-descanned photomultiplier tubes. EGFP and DsRed were excited at 920 nm, EYFP and TRITC at 880 nm, and fluorescent probes at 800 nm. For four-dimensional datasets, three-dimensional stacks were captured every 30–45 s for 30–90 min. Raw imaging data were processed with Imaris 7 (Bitplane). Autofluorescence was removed via channel arithmetic function from Imaris XT (Bitplane). Cellular motion was tracked semi-automatically via built-in tracking functions aided by manual corrections. For tracking contact duration, spots and surfaces were generated for T cells and $TRITC^+$ cells, respectively, and were tracked with custom MATLAB scripts interfaced with Imaris XT. Movies were generated in Imaris and composed in After Effects (Adobe). See also Supplemental Experimental Procedures.

Imaging Thick LN Sections

Harvested LNs were either fixed in PLP for 2–6 hr or left unfixed, prior to embedding in 2% agarose. Agarose blocks containing tissues were sliced using a VT1200 S vibratome (Leica Biosystems) into 200–250 μm thick sections. For antibody staining, tissue sections were blocked for 1.5–2 hr before incubating with antibodies for 8–16 hr at 4°C. Sections were mounted on glass slides and images were acquired on a LSM710 NLO multiphoton microscope (Carl Zeiss). Post-acquisition processing was performed in Imaris (Bitplane). For cluster detection, spots were created with built-in spot detection function in Imaris and clusters detected with custom MATLAB scripts interfaced with Imaris XT. A cluster was defined as a minimum of 3 cells aggregating within a distance of 15 μm measured from the centroid of each cell. See also Supplemental Experimental Procedures.

Statistics

Comparison of data sets was performed using one-way analysis of variance with Tukey's post-test or two-tailed, paired t test where appropriate.

SUPPLEMENTAL INFORMATION

Supplemental Information includes five figures, seven movies, and Supplemental Experimental Procedures and can be found with this article online at http://dx.doi.org/10.1016/j.immuni.2015.07.020.

AUTHOR CONTRIBUTIONS

J.L.H. performed all imaging experiments; J.L.H., P.G.W., and A.Z. performed experiments and analyzed data; A.G.B., W.R.H., and S.N.M. designed the research and interpreted data; J.L.H. and S.N.M. prepared figures and movies; and S.N.M. wrote the manuscript.

ACKNOWLEDGMENTS

We thank S. Bedoui for discussions and C. Jones, G. Davey, and M. Damtsis for technical assistance. Supported by the National Health and Medical Research Council of Australia (P.G.W., A.G.B., W.R.H., and S.N.M.) and the Australian Research Council (W.R.H. and S.N.M.).

Received: May 9, 2015
Revised: June 16, 2015
Accepted: June 23, 2015
Published: August 18, 2015

REFERENCES

Allan, R.S., Smith, C.M., Belz, G.T., van Lint, A.L., Wakim, L.M., Heath, W.R., and Carbone, F.R. (2003). Epidermal viral immunity induced by $CD8alpha^+$ dendritic cells but not by Langerhans cells. Science *301*, 1925–1928.

Allan, R.S., Waithman, J., Bedoui, S., Jones, C.M., Villadangos, J.A., Zhan, Y., Lew, A.M., Shortman, K., Heath, W.R., and Carbone, F.R. (2006). Migratory dendritic cells transfer antigen to a lymph node-resident dendritic cell population for efficient CTL priming. Immunity *25*, 153–162.

Bedoui, S., Whitney, P.G., Waithman, J., Eidsmo, L., Wakim, L., Caminschi, I., Allan, R.S., Wojtasiak, M., Shortman, K., Carbone, F.R., et al. (2009). Cross-presentation of viral and self antigens by skin-derived $CD103^+$ dendritic cells. Nat. Immunol. *10*, 488–495.

Belz, G.T., Smith, C.M., Eichner, D., Shortman, K., Karupiah, G., Carbone, F.R., and Heath, W.R. (2004a). Cutting edge: conventional CD8 $alpha^+$ dendritic cells are generally involved in priming CTL immunity to viruses. J. Immunol. *172*, 1996–2000.

Belz, G.T., Smith, C.M., Kleinert, L., Reading, P., Brooks, A., Shortman, K., Carbone, F.R., and Heath, W.R. (2004b). Distinct migrating and nonmigrating dendritic cell populations are involved in MHC class I-restricted antigen presentation after lung infection with virus. Proc. Natl. Acad. Sci. USA *101*, 8670–8675.

Belz, G.T., Shortman, K., Bevan, M.J., and Heath, W.R. (2005). $CD8alpha^+$ dendritic cells selectively present MHC class I-restricted noncytolytic viral and intracellular bacterial antigens in vivo. J. Immunol. *175*, 196–200.

Braun, A., Worbs, T., Moschovakis, G.L., Halle, S., Hoffmann, K., Bölter, J., Münk, A., and Förster, R. (2011). Afferent lymph-derived T cells and DCs use different chemokine receptor CCR7-dependent routes for entry into the lymph node and intranodal migration. Nat. Immunol. *12*, 879–887.

Carrasco, Y.R., and Batista, F.D. (2007). B cells acquire particulate antigen in a macrophage-rich area at the boundary between the follicle and the subcapsular sinus of the lymph node. Immunity *27*, 160–171.

Castellino, F., Huang, A.Y., Altan-Bonnet, G., Stoll, S., Scheinecker, C., and Germain, R.N. (2006). Chemokines enhance immunity by guiding naive $CD8^+$ T cells to sites of $CD4^+$ T cell-dendritic cell interaction. Nature *440*, 890–895.

Coles, R.M., Mueller, S.N., Heath, W.R., Carbone, F.R., and Brooks, A.G. (2002). Progression of armed CTL from draining lymph node to spleen shortly after localized infection with herpes simplex virus 1. J. Immunol. *168*, 834–838.

Crozat, K., Tamoutounour, S., Vu Manh, T.P., Fossum, E., Luche, H., Ardouin, L., Guilliams, M., Azukizawa, H., Bogen, B., Malissen, B., et al. (2011). Cutting edge: expression of XCR1 defines mouse lymphoid-tissue resident and migratory dendritic cells of the CD8α^+ type. J. Immunol. *187*, 4411–4415.

Dorner, B.G., Dorner, M.B., Zhou, X., Opitz, C., Mora, A., Güttler, S., Hutloff, A., Mages, H.W., Ranke, K., Schaefer, M., et al. (2009). Selective expression of the chemokine receptor XCR1 on cross-presenting dendritic cells determines cooperation with CD8$^+$ T cells. Immunity *31*, 823–833.

Edelson, B.T., Kc, W., Juang, R., Kohyama, M., Benoit, L.A., Klekotka, P.A., Moon, C., Albring, J.C., Ise, W., Michael, D.G., et al. (2010). Peripheral CD103$^+$ dendritic cells form a unified subset developmentally related to CD8alpha$^+$ conventional dendritic cells. J. Exp. Med. *207*, 823–836.

Eidsmo, L., Stock, A.T., Heath, W.R., Bedoui, S., and Carbone, F.R. (2012). Reactive murine lymph nodes uniquely permit parenchymal access for T cells that enter via the afferent lymphatics. J. Pathol. *226*, 806–813.

Gebhardt, T., Whitney, P.G., Zaid, A., Mackay, L.K., Brooks, A.G., Heath, W.R., Carbone, F.R., and Mueller, S.N. (2011). Different patterns of peripheral migration by memory CD4$^+$ and CD8$^+$ T cells. Nature *477*, 216–219.

Gerner, M.Y., Torabi-Parizi, P., and Germain, R.N. (2015). Strategically localized dendritic cells promote rapid T cell responses to lymph-borne particulate antigens. Immunity *42*, 172–185.

Heath, W.R., and Carbone, F.R. (2009). Dendritic cell subsets in primary and secondary T cell responses at body surfaces. Nat. Immunol. *10*, 1237–1244.

Hickman, H.D., Takeda, K., Skon, C.N., Murray, F.R., Hensley, S.E., Loomis, J., Barber, G.N., Bennink, J.R., and Yewdell, J.W. (2008). Direct priming of antiviral CD8$^+$ T cells in the peripheral interfollicular region of lymph nodes. Nat. Immunol. *9*, 155–165.

Hickman, H.D., Li, L., Reynoso, G.V., Rubin, E.J., Skon, C.N., Mays, J.W., Gibbs, J., Schwartz, O., Bennink, J.R., and Yewdell, J.W. (2011). Chemokines control naive CD8$^+$ T cell selection of optimal lymph node antigen presenting cells. J. Exp. Med. *208*, 2511–2524.

Hildner, K., Edelson, B.T., Purtha, W.E., Diamond, M., Matsushita, H., Kohyama, M., Calderon, B., Schraml, B.U., Unanue, E.R., Diamond, M.S., et al. (2008). Batf3 deficiency reveals a critical role for CD8alpha$^+$ dendritic cells in cytotoxic T cell immunity. Science *322*, 1097–1100.

Igyártó, B.Z., Haley, K., Ortner, D., Bobr, A., Gerami-Nejad, M., Edelson, B.T., Zurawski, S.M., Malissen, B., Zurawski, G., Berman, J., and Kaplan, D.H. (2011). Skin-resident murine dendritic cell subsets promote distinct and opposing antigen-specific T helper cell responses. Immunity *35*, 260–272.

Itano, A.A., McSorley, S.J., Reinhardt, R.L., Ehst, B.D., Ingulli, E., Rudensky, A.Y., and Jenkins, M.K. (2003). Distinct dendritic cell populations sequentially present antigen to CD4 T cells and stimulate different aspects of cell-mediated immunity. Immunity *19*, 47–57.

Junt, T., Moseman, E.A., Iannacone, M., Massberg, S., Lang, P.A., Boes, M., Fink, K., Henrickson, S.E., Shayakhmetov, D.M., Di Paolo, N.C., et al. (2007). Subcapsular sinus macrophages in lymph nodes clear lymph-borne viruses and present them to antiviral B cells. Nature *450*, 110–114.

Kastenmüller, W., Brandes, M., Wang, Z., Herz, J., Egen, J.G., and Germain, R.N. (2013). Peripheral prepositioning and local CXCL9 chemokine-mediated guidance orchestrate rapid memory CD8+ T cell responses in the lymph node. Immunity *38*, 502–513.

Kim, T.S., and Braciale, T.J. (2009). Respiratory dendritic cell subsets differ in their capacity to support the induction of virus-specific cytotoxic CD8$^+$ T cell responses. PLoS ONE *4*, e4204.

Kissenpfennig, A., Henri, S., Dubois, B., Laplace-Builhé, C., Perrin, P., Romani, N., Tripp, C.H., Douillard, P., Leserman, L., Kaiserlian, D., et al. (2005). Dynamics and function of Langerhans cells in vivo: dermal dendritic cells colonize lymph node areas distinct from slower migrating Langerhans cells. Immunity *22*, 643–654.

Kumamoto, Y., Mattei, L.M., Sellers, S., Payne, G.W., and Iwasaki, A. (2011). CD4$^+$ T cells support cytotoxic T lymphocyte priming by controlling lymph node input. Proc. Natl. Acad. Sci. USA *108*, 8749–8754.

Lee, H.K., Zamora, M., Linehan, M.M., Iijima, N., Gonzalez, D., Haberman, A., and Iwasaki, A. (2009). Differential roles of migratory and resident DCs in T cell priming after mucosal or skin HSV-1 infection. J. Exp. Med. *206*, 359–370.

Merad, M., Sathe, P., Helft, J., Miller, J., and Mortha, A. (2013). The dendritic cell lineage: ontogeny and function of dendritic cells and their subsets in the steady state and the inflamed setting. Annu. Rev. Immunol. *31*, 563–604.

Miller, M.J., Wei, S.H., Cahalan, M.D., and Parker, I. (2003). Autonomous T cell trafficking examined in vivo with intravital two-photon microscopy. Proc. Natl. Acad. Sci. USA *100*, 2604–2609.

Mueller, S.N., Heath, W., McLain, J.D., Carbone, F.R., and Jones, C.M. (2002a). Characterization of two TCR transgenic mouse lines specific for herpes simplex virus. Immunol. Cell Biol. *80*, 156–163.

Mueller, S.N., Jones, C.M., Smith, C.M., Heath, W.R., and Carbone, F.R. (2002b). Rapid cytotoxic T lymphocyte activation occurs in the draining lymph nodes after cutaneous herpes simplex virus infection as a result of early antigen presentation and not the presence of virus. J. Exp. Med. *195*, 651–656.

Mueller, S.N., Jones, C.M., Chen, W., Kawaoka, Y., Castrucci, M.R., Heath, W.R., and Carbone, F.R. (2003). The early expression of glycoprotein B from herpes simplex virus can be detected by antigen-specific CD8$^+$ T cells. J. Virol. *77*, 2445–2451.

Nakanishi, Y., Lu, B., Gerard, C., and Iwasaki, A. (2009). CD8(+) T lymphocyte mobilization to virus-infected tissue requires CD4(+) T-cell help. Nature *462*, 510–513.

Phan, T.G., Grigorova, I., Okada, T., and Cyster, J.G. (2007). Subcapsular encounter and complement-dependent transport of immune complexes by lymph node B cells. Nat. Immunol. *8*, 992–1000.

Qi, H., Egen, J.G., Huang, A.Y.C., and Germain, R.N. (2006). Extrafollicular activation of lymph node B cells by antigen-bearing dendritic cells. Science *312*, 1672–1676.

Ridge, J.P., Di Rosa, F., and Matzinger, P. (1998). A conditioned dendritic cell can be a temporal bridge between a CD4$^+$ T-helper and a T-killer cell. Nature *393*, 474–478.

Schnorrer, P., Behrens, G.M., Wilson, N.S., Pooley, J.L., Smith, C.M., El-Sukkari, D., Davey, G., Kupresanin, F., Li, M., Maraskovsky, E., et al. (2006). The dominant role of CD8$^+$ dendritic cells in cross-presentation is not dictated by antigen capture. Proc. Natl. Acad. Sci. USA *103*, 10729–10734.

Singh-Jasuja, H., Thiolat, A., Ribon, M., Boissier, M.C., Bessis, N., Rammensee, H.G., and Decker, P. (2013). The mouse dendritic cell marker CD11c is down-regulated upon cell activation through Toll-like receptor triggering. Immunobiology *218*, 28–39.

Smith, C.M., Wilson, N.S., Waithman, J., Villadangos, J.A., Carbone, F.R., Heath, W.R., and Belz, G.T. (2004). Cognate CD4(+) T cell licensing of dendritic cells in CD8(+) T cell immunity. Nat. Immunol. *5*, 1143–1148.

Stock, A.T., Mueller, S.N., van Lint, A.L., Heath, W.R., and Carbone, F.R. (2004). Cutting edge: prolonged antigen presentation after herpes simplex virus-1 skin infection. J. Immunol. *173*, 2241–2244.

van Lint, A., Ayers, M., Brooks, A.G., Coles, R.M., Heath, W.R., and Carbone, F.R. (2004). Herpes simplex virus-specific CD8$^+$ T cells can clear established lytic infections from skin and nerves and can partially limit the early spread of virus after cutaneous inoculation. J. Immunol. *172*, 392–397.

Weeks, B.S., Ramchandran, R.S., Hopkins, J.J., and Friedman, H.M. (2000). Herpes simplex virus type-1 and -2 pathogenesis is restricted by the epidermal basement membrane. Arch. Virol. *145*, 385–396.

Wiesel, M., and Oxenius, A. (2012). From crucial to negligible: functional CD8$^+$ T-cell responses and their dependence on CD4$^+$ T-cell help. Eur. J. Immunol. *42*, 1080–1088.

Zhao, X., Deak, E., Soderberg, K., Linehan, M., Spezzano, D., Zhu, J., Knipe, D.M., and Iwasaki, A. (2003). Vaginal submucosal dendritic cells, but not Langerhans cells, induce protective Th1 responses to herpes simplex virus-2. J. Exp. Med. *197*, 153–162.